

A 7.5mm Steiner chain fiber-optic system for multi-segment flex sensing

S. Sareh, Y. Noh, T. Ranzani, H. Wurdemann, H. Liu, K. Althoefer, *Member, IEEE*

Abstract— this paper presents an extensible highly compact fiber-optic system for multi-segment flex sensing. This fiber-optic arrangement is 7.5 mm in diameter and is comprised of a flexible and stretchable Steiner chain ($n=12$) housing at the top which accommodates passive cables used for sensing, followed by a basal rigid fiber-optic sensing unit. The U-shape loopback design of the sensing system allows integration of electronics on one side and away from the sensing region. A low-friction retractable distance modulation array is designed and implemented to reduce the hysteresis and recover reference sensor values when the arm returns to its original straight configuration. This sensing system is able to measure the dynamic flex patterns of the actuation system to which it conforms. This sensing system can also be embedded inside soft robotic manipulators for multi-segment flex sensing independent of actuation systems, temperature or external load from the environment. This arrangement can also be used as a complete manipulation system when actuating tendons are attached.

I. INTRODUCTION

Sensing technologies suitable for integrating into the new highly redundant [1], [2] and soft [3], [4], class of robotic manipulators are becoming increasingly demanded, due to the inclusive nature of these manipulation systems enabling medical [5], [6], [7] and robotic [8], [9] applications in confined space. These robotic systems are usually made from mutually-tangent curved segments enabling high degrees of robotic articulation in unstructured and cluttered workspaces [4]. The piecewise bendable and extensible segments of these soft robotic systems enables reaching targets which are prohibited by conventional rigid manipulators, however, control of these robotic manipulators requires precise shape sensing which is achievable through multi-segment flex sensing.

The complex motion patterns generated by these robots have been mainly tracked through incorporation of vision systems [10] and electromagnetic tracking [11] especially in medical applications. However the visual techniques are often restricted with visual occlusion and electromagnetic tracking is subject to magnetic field distortions and have limitations with regards to mobility of the magnetic field generation system.

There are various ways of sensing flexion through passive resistive devices made from conductive inks and fabrics, e.g. the off-the-shelf Flexpoint sensor (Flexpoint Sensor Systems,

Inc, USA), and specific types of bipolar smart materials, e.g. Ionic Polymer Metal Composites (IPMCs) [12], however, they are usually not suitable for three dimensional sensing. Fiber Bragg Grating (FBG) shape sensing tubes were proposed for shape sensing in continuum robots. The FBG sensors are highly sensitive to the change in environmental temperature and strain. In the case of a non-uniform strain field the strain compensation is complex [13], [14]. Shape sensing based on FBG is not suitable for extensible systems. Light intensity modulation [15], [16] is another optical approach that can be adapted for flex sensing [17]. This approach is temperature independent [17], and low-cost. In this paper, we present the design and development of an extensible multi-segment flex sensor based on light intensity modulation between two optical fiber tips. In the following, we explain the design, fabrication and calibration of the sensor device, and subsequent preliminary experimental studies.

II. DESIGN OF THE FLEX SENSING SYSTEM

The flex sensing system comprised of a Steiner chain flexible section with embedded passive cables at the distal side, and a distance modulation array at the proximal side, as shown in Figure 1.

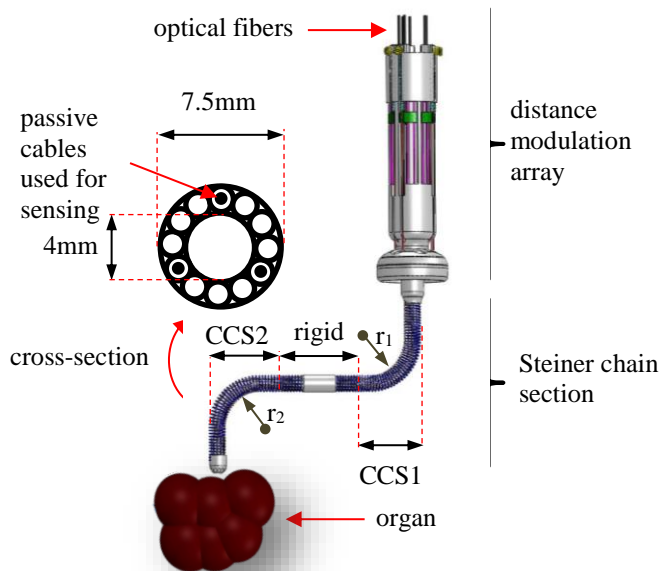


Figure 1. The overall structure of the flex sensing system comprising of a six-channel distance modulation array and a flexible Steiner chain section. Note that the flexible section also provides an empty central channel for end-effector instruments (CCS1 and CCS2 indicate constant curvature segments with radii of r_1 and r_2 , respectively).

The research leading to these results has received funding from the European Commission's Seventh Framework Programme; project STIFF-FLOP (Grant No: 287728).

S. Sareh, Y. Noh, H. Wurdemann, H. Liu, and K. Althoefer are with Centre for Robotics Research, King's College London, UK.

Tommaso Ranzani is with the Bio-Robotics Institute, Scuola Superiore Sant'Anna, Italy.
(corresponding author: sina.sareh@kcl.ac.uk).

Whilst the Steiner chain section is responsible for maintaining the radial distance between passive cables and the center of the flexible arm during manipulations, the distance modulation array couples the motion of passive cables with light-emitting optical fibers using a low-friction sliding mechanism at the base. Each Light-emitting optical fiber is paired and aligned with an optical detector fixed at the base.

The flex sensing principle explained above employs multiple passive cables passed through tiny spring channels (1.2 mm outer diameter) along the length of the arm (50 mm in length). These channels are located at the same distance from the central axis of the manipulator (a design parameter ‘ d ’) but using different equally spaced angular positions. The cable channels are accordingly extended outside the manipulator using the 3D printed part of the sensor where they are converted to sliding rails. A very low friction mechanism was developed for sliding which employs two steel needles with thickness of 0.89 mm located in parallel and 4mm away from each other. A specialized v-shaped mechano-optical coupler, the interface between passive cables of the Steiner chain section and optical fibers of the distance modulation array, was designed and fabricated to be able to smoothly slide around needles and carry the light-transmitting optical fibers inside the sensor base. The sliding plate is linked with a 2mm outer diameter extension spring (fixed at one side), to be retracted and recovered after being pulled by cables. This allows the flex sensor to exploit a retractable sliding mechanism for modulating the distance between emitter and detector optical fibers. When the arm undergoes a bending deformation, the fed length of the cables (the length portion inside the arm) changes. These changes in the length of equally spaced cables modulate the position of the transmitting optical fibers and, hence, the received light intensity by detectors (e.g. KEYENCE™ Digital Fiber Optic Sensor). The received light is then converted into digital information. This principle was used for the computation of the bending curvature of the arm.

A. The Steiner Chain section

In geometry, a Steiner chain is a set of mutually tangent n circles, all of which are tangent to two given non-intersecting circles, just like the structure illustrated in Figure 2a. The Steiner chain mathematics can represent the design of a steerable endoscope in [19]. In this design, low-cost commercial springs are tangentially combined in parallel to tightly accommodate driving tendons and prevent their radial displacement. Figure 2a can also explain the cross section of such actuation mechanism. Clearly, this structure can house also passive cables to code the shape of the endoscope or similar manipulation systems. Hence, we would like to incorporate this analogy to come up with a more systematic design approach.

The flex sensor of each segment of the arm consists of three passive cables with fed length, the extended length portion of the cable pulled into the flexible arm in response to a bending deformation or elongation, of s_1 , s_2 , and s_3 . These passive cables are sliding inside flexible Steiner chain housings in the periphery of the arm, in parallel with driving tendons. In

response to a specific amount of bending deformation in a particular orientation, there is a unique distance matrix of $s=[s_1 s_2 s_3]$ which can describe bending angle and orientation of the arm. Figure 2b shows the configuration of a flexible arm in the 3D space [18].

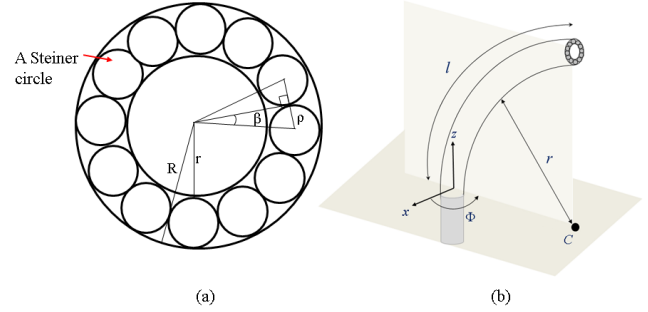


Figure 2. (a) The Steiner chain cross-section of the arm, (b) The flexed configuration and associated parameters in 3D [18].

The fed length of cables in the periphery of the arm s_i can be calculated as

$$s_i = f_i + L \quad (2)$$

where L is the passive length of each segment (here: $L=30\text{mm}$), and f_i is the change in this value due to a bending deformation, and i is the cable number. The length of the central axis of the each segment can be obtained through,

$$S = \frac{1}{3} \sum_{i=1}^3 (s_i) \quad (3)$$

and the bending angle θ can be computed as

$$\theta = \frac{S - s_1}{d \cdot \cos(\frac{\pi}{2} - \varphi)} \quad (4)$$

where φ is the end orientation of the segment, and is expressed as

$$\varphi = \tan^{-1} \left(\frac{\sqrt{3}(s_2 + s_3 - 2s_1)}{3(s_2 - s_3)} \right) \quad (5)$$

Variable d in equation (4) describes the distance between the central axis of the manipulator and the parallel passive cables. In the following, we show that the change in the fed length of cables in the periphery of the arm ($\Delta s_{i,m}$, where m is the state indicator: $m=1$ for the primary and $m=2$ for the secondary state) is in direct relationship with d . Therefore this parameter is directly affecting the resolution of the sensor system.

By substituting $\varphi_m = \frac{\pi}{2}$ and a very small amount of bending $\theta_m = \frac{\pi}{180}$ in equations (5) and then (4)

$$-2s_{1,1} + s_{2,1} + s_{3,1} = 0.0525d \quad (6)$$

where $s_{i,1}$ denotes the primary fed length of the cables s_i . Also from equation (5), $s_{2,1} = s_{3,1}$, therefore

$$s_{2,1} - s_{1,1} = 0.0262d \quad (7)$$

If substituting $\varphi_m = \frac{\pi}{2}$ and $\theta_m = \frac{\pi}{2}$ in the same set of equations

$$s_{2,2} - s_{1,2} = \frac{3\pi}{4}d \quad (8)$$

where $s_{i,2}$ explains the secondary fed length of the cable s_i . Therefore the total change in the fed length for the cable s_1 can be obtained by subtracting equations (7) and (8)

$$\Delta s_1 = s_{2,2} - s_{1,2} - s_{2,1} + s_{1,1} \quad (9)$$

The arm segments are made from extension springs and therefore are incompressible. Assuming $s_{2,2} \approx s_{2,1}$, the change in the cable's fed length can be calculated through

$$\Delta s_1 \approx \frac{3\pi}{4}d \quad (10)$$

The KEYENCE™ Digital Fiber Optic Sensor used in this study can effectively measure a maximum length change of 20 mm. Therefore, in order to measure a 90° bending deformation, the maximum value of d must not exceed 8.4mm. It is clear that for measuring a maximum of 180° bending, which can be regarded as two successive 90° bending as targeted in this study, this value should be reduced to 4.2mm. Since the maximum combined deformation of the two segments should be also measureable within this 20mm range, d_{\max} needs to be 2.1mm.

To preserve the maximum resolution of the sensing system, we opt for the maximum value for d , which is 2.1mm (as explained above). This necessitates incorporating an inner spring with a diameter of slightly less than 4mm. We have, therefore used LEM050AB 05 S stainless steel extension spring (Lee Spring Ltd., USA) with outer diameter of 3.505 mm and wire diameter of 0.508 as the central spine. For Steiner springs (corresponds with an Steiner circle on the cross-section view, Figure 3), we have used custom springs with an outer diameter of 1.2mm and a wire diameter of 0.25mm, as they were available in our laboratory. Therefore steel passive cables with diameter of 0.27mm (Carl Stahl Ltd., Germany) can be radially fixed at approximately $d=2.1$ mm away from the centre, and the central angle $\beta = \sin^{-1}\left(\frac{\rho}{r+\rho}\right)$ can be calculated as approximately 15°. Hence, the number of Steiner springs is $n = \frac{180}{\beta} = 12$ and the inner diameter of the outer spring should be approximately $R = r + 2\rho = 5.91$ mm. We have, therefore, selected LEM070CB 05 S (Lee Spring Ltd., USA) with an outer diameter of 7.49mm and a wire diameter of 0.711mm.

Therefore, the tip section of the sensing system comprised of twelve Steiner channels. The design uses three of them for sensing, these channels pass through the whole length of the two segment arm and house sensing wires, and considers six channels to accommodate six driving tendons. Therefore three channels are empty and can be used for other applications, e.g. end-effector wiring.

B. Design of a low-friction retractable distance modulation array

In response to a bending deformation, the portion of length of each optical fiber, which is fed peripherally into the periphery of the flexible arm, changes. When the arm returns to its original straight configuration, fiber's fed lengths are also required to follow back to the original. Several reasons including friction, and hysteresis in the mechanical structure and material properties prevent fulfilling this essential condition and introduce malfunction into the sensory system. In order to make sure the mutual distance between the emitting and detecting fiber optic pairs is recovered, a spring returning mechanism is a very natural solution. In addition, we need to couple the passive cables that are passed through the length of the flexible arm with fiber optic pairs for distance measurement using KEYENCE™ sensors. This mechanism must produce minimal friction to be able to perform the expected role within the sensory system.

1) Loopback design of the optical system

The commercial off-the-shelf stretch (length) sensors, e.g. stretch sensors from StretchSense Ltd, New Zealand, and PolyPower® Stretch Sensors, are usually fabricated to be free from electronics at one end. This free end is usually coupled with the moving end of the actuator to measure the length change. Similarly, here, it is not ideal to have the emitter and the detector at opposite sides of the sensing media. In order to allow all the electronics to be at one end of the sensor we employed a U-shape arrangement of optical fibers to produce a loopback configuration. This enables placing the emitter and detector next to each other, as illustrated in Figure 3(b).

2) The Steel spring-needle double slider

A low-friction sliding mechanism is also essential to enable modulating the mutual distance between any pair of optical fibers. In order to address this requirement, we have fabricated a highly smooth double slider using two steel needles (44mm length x 0.86mm diameter, John James Needles, Worcestershire, England), surrounded by two small-sized pieces of steel springs (1.4 mm outer diameter, 0.2 mm wire diameter), that are anchored in parallel and 4mm away from each other into the plastic sensor base. Each steel spring that is able to smoothly slide around the surrounded needle, is embedded into a v-shaped plastic mechano-optical coupler. Each coupler links a passive cable with its corresponding fiber optic pair. This mechanism is shown in Figure 3(d). Figure 3(c) illustrates the cross-section of the distance modulation array with its maximum outer diameter of 22 mm.

I. FABRICATION AND ASSEMBLY

The sensorized arm in its finished configuration is shown in Figure 4(a), and 4(b). The off-robot structure of the mechano-optical coupler is demonstrated in Figure 4(c), comprising of a v-shaped 3D printed part with an U-shaped housing for an optical fiber, and a connection module which links a 2 mm outer diameter extension spring (Lee Spring Ltd., USA), with a 0.27 mm thick steel wire rope (Carl Stahl, Germany), used

as the passive cable. Note that these 2 mm extension springs are responsible for cables position recovery and therefore we call them recovery springs. We have considered an initial stretch of 5 mm in recovery springs to increase the pulling force. Finally, Figures 4(d) and (e) present the fully assembled structure of the main top (Steiner chain), and the bottom (distance modulation array) parts of the arm. All plastic parts were fabricated using a rapid prototyping machine (Project HD-3000 Plus, 3D Systems).

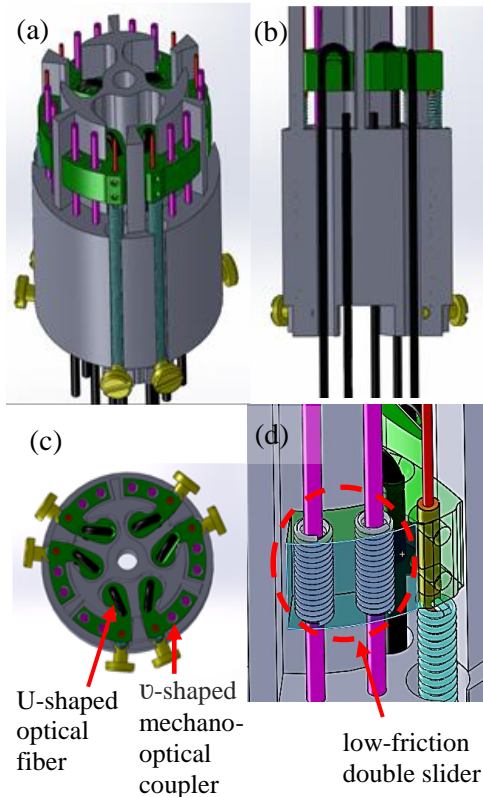


Figure 3. The CAD designs of the multi-segment flex sensor exhibiting integrated technologies: (a) the side view showing the elastic recovery mechanism of the slider, (b) the low-friction steel spring-double needle sliding mechanism to maintain the direction of the motion, (c) the U-shape fiber optic arrangement.

II. EXPERIMENTAL CALIBRATION AND FLEX SENSING VALIDATION

In order to validate the design and implementation of the two-segment flex sensor, we have performed a set of experiments where either one or both segments were actuated at time. Two HD cameras were placed at the top and side of the manipulator to record ground truth shape information. The present manipulation platform is not yet equipped with motors or other actuators. So we attached the middle and tip of the arm to fixed points on the wall, using steel wires, in order to generate stable shape patterns. Subsequently we have recorded the light intensity (and corresponding voltage) values from KEYENCE™ Fiber-Optic Sensors and cameras.

To convert voltage values to corresponding values of distance between optical fiber tips, we have extracted the calibration relationship for all six fiber optic channels. The

averaged calibration data, presented together with error bars in Figure 5, was splined in MATLAB (MathWorks, Inc., Natick, MA) to form the calibration curve.

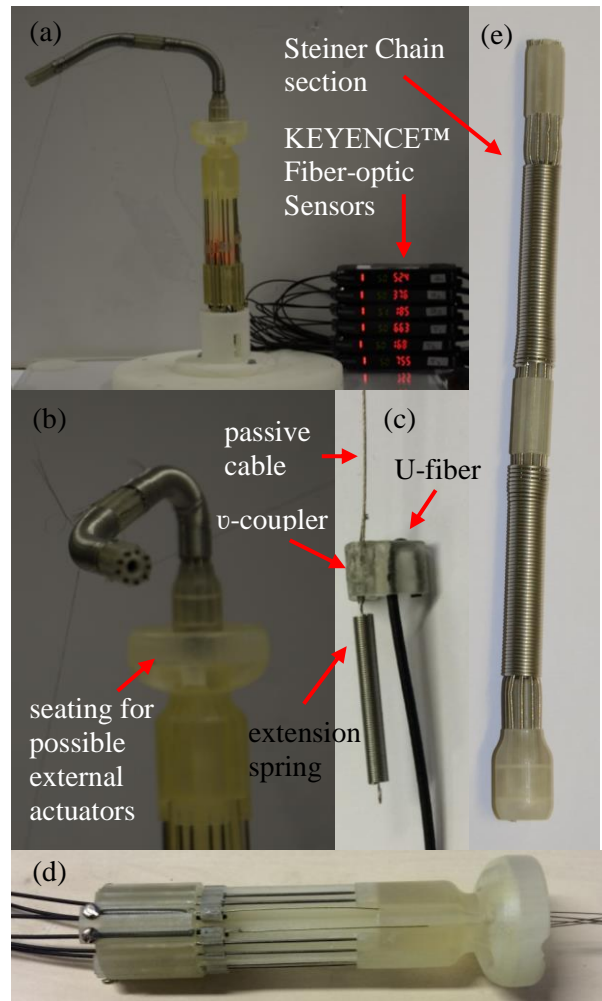


Figure 4. The prototype of the arm and sensing system: (a) the finished configuration of the sensorized manipulation system, (b) close-up view of the top part, (c) the v-shaped mechano-optical coupler, (d) the fully assembled structure of the distance modulation array, and (e) the structure of the Steiner Chain section.

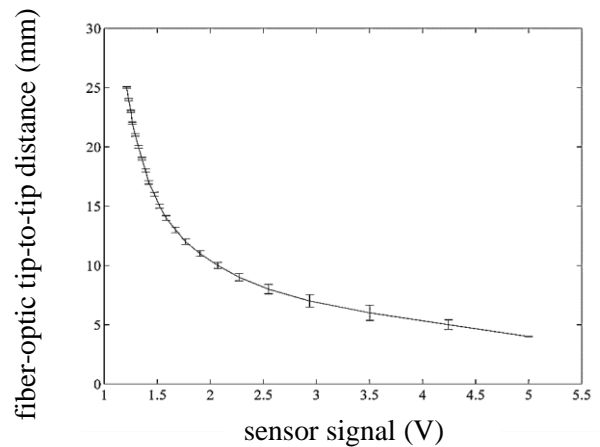


Figure 5. The averaged calibration curve and error bars.

Having calibrated the sensors, the manipulator was forced into various three dimensional shapes, shown in Figure 6 and the sensor signals were recorded and analyzed.

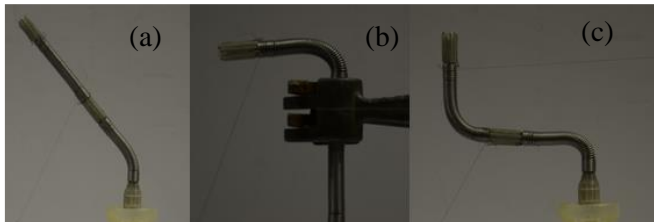


Figure 6. Examples of key experimental configurations: (a) independent activation of base segment, (b) independent activation of the tip segment (note that the intersegment link is clamped to produce a stationary base), and (c) simultaneous activation of two segments.

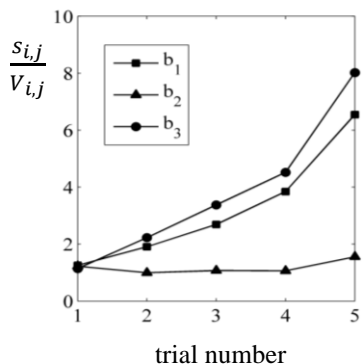


Figure 7. The voltage-distance relationship for the base segment experiment.

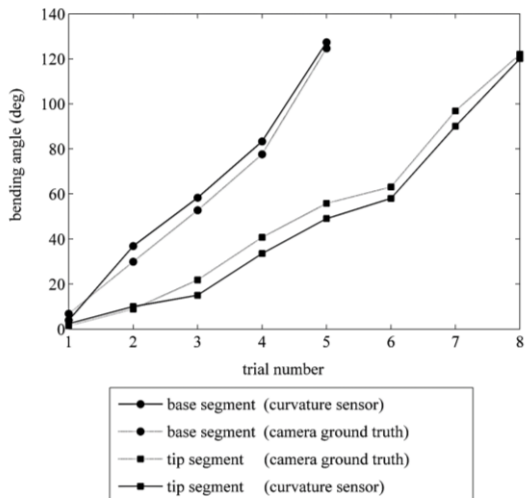


Figure 8. The experimental results of flex sensing in individual segments.

In order to use the constant curvature bending model, the acquired voltage signals were fed into the splined calibration data presented in Figure 5 to back-calculate the tip-to-tip fiber optic distances. Subsequently, these distances were substituted into equations (4) and (5) to calculate the bending curvature and orientation of the manipulator. Figure 8 shows the experimental results compared with their corresponding ground truth information extracted from camera images using a custom MATLAB (MathWorks, Inc., Natick, MA) code.

In Figure 7, $S_{i,j}$ represents the tip-to-tip distance between optical fiber pair, where $i=\{1,2,3\}$ is the pair number and $j=\{1,2,3,4,5\}$ is the trial number. The trend in $s_{i,j}/V_{i,j}$ implies that the arm was flexed approximately symmetric with respect to cables b_1 and b_3 , where these two cables are virtually stretched (physically only the fed length of cables can change). The cable b_2 was only slightly compressed, with respect to the length change in other two cables which confirms the design assumption led to equation (10).

Figure 8 shows the experimental results, where segments of the arm were actuated individually, implying a maximum tracking error of around 7° in tip segment when the arm was flexed with ground truth value of 40° . This error was decreased to 5° as the arm reached a ground truth bending angle of 63° and around 2° for ground truth value of 122° . A similar behavior can be seen in the flex data, also presented in figure 8, of the base segment. The finer behavior of the sensor for large flexions, can be due to better positioning of cables inside the spring channels. These channels have an internal diameter of around 0.8mm and are housing two 0.27 mm thick cables, along the length of the base segment and only one of them along the length of the tip segment. So there is some room for cables to play radially, if they are not pulled tightly using extension springs. However, we have considered a pre-stretch of 5mm in the design, the experimental results implies that the error can be reduced if this initial stretch is increased.

III. CALCULATION OF THE BENDING CURVATURE IN A TWO-SEGMENT ARM BASED ON COLLOCATED CABLES

In order to simplify the multi-segment curvature sensing, this work exploits a method which we call ‘‘collocated cables’’. As mentioned in section II.A this sensing arrangement uses only three Steiner channels out of twelve for sensing. There are two passive cables sliding inside each of these three channels; one fixed between two segments and the other one at the tip of the manipulator. This allows measuring the bending angle in multi-segment arms in a modular way (with minimal amendment in cables’ length computation explained in the following). When the arm undergoes a complex two-segment movement, the change in the length of cables passing through the whole length of the arm to the tip (t-type cables t_1 , t_2 , and t_3), is only partially due to the bending of the tip segment. However, the change in the length of the fibers fixed at the tip of the base segment (b-type cables b_1 , b_2 , and b_3) is purely due to the bending in this segment. In our sensing arrangement, each t-type cable is accompanied by a b-type cable, as shown in Figure 9. This allows calculating the share of each segment from the total length change.

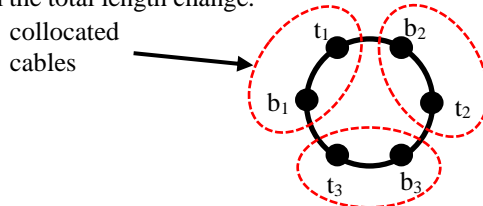


Figure 9. The cross-section of the distance modulation array, showing the collocated arrangement of passive cables used for sensing.

To intuitively evaluate this method, we moved segments of the arm into a complex S-shape configuration, shown in Figure 6(c). Using camera ground truth information, we have calculated the bending angle in two segments as $\theta_{\text{Ground},1}=91.2^\circ$, $\theta_{\text{Ground},2}=95.1^\circ$.

Table 1 summarizes the calculation of length change in each segment based on collocated cables' lengths; V_{bi} values, $i=\{1,2,3\}$, represent KEYENCE voltage readings associated with cables that are fixed between two segments; V_{ti} are readings associated with cables passed through the whole length of the arm and fixed at the tip. Mapping into the splined voltage-distance relationship, Figure 5, corresponding fibers' mutual distances s_{bi} and s_{ti} are calculated. Whilst values of s_{bi} are representing the pure length change in the base segment, the pure length change of the tip segment can be computed through $s_{pi}=s_{ti}-s_{bi}$.

Table 1. Calculation of the pure length change in each segment based on collocated cables approach.

Voltage (V)	V_{b1}	V_{b2}	V_{b3}	V_{t1}	V_{t2}	V_{t3}
	3.99	2.92	1.93	1.89	2.27	1.93
Length (mm)	s_{b1}	s_{b2}	s_{b3}	s_{t1}	s_{t2}	s_{t3}
	5.34	7.04	10.87	11.11	9.01	10.87
Length (mm)	s_{p1}		s_{p2}		s_{p3}	
	5.77		1.96		0	

By substituting pure distance values into equations (3) to (5), the sensory bending angles are computed as $\theta_{\text{Sensor},1}=89.2^\circ$ and $\theta_{\text{Sensor},2}=92.4^\circ$. This implies an error of less than 3° in each segment.

IV. CONCLUSIONS AND FUTURE WORKS

In this paper, we have presented the design and fabrication of a flex sensing system for a 7.5mm multi-segment flexible manipulation arm. Starting from theoretical design, we have optimised the radial location of the passive cables used for sensing along the periphery of the arm in order to represent a trade-off between maximum compactness of the sensing system and using the full capacity of the optical measurement system in terms of the measurement resolution. In the next step, we have presented a Steiner Chain design ($n=12$) for the flexible part of the sensor system. Three out of twelve Steiner Chain channels were used for flex sensing in the two-segment flexible arm. Subsequently we have designed and fabricated a low-friction fiber-optic distance modulation array based on a new spring-needle double slider to precisely measure the change in the length of cables which are embedded in the periphery of the arm during flexion. The design also employs a loopback optical method to keep all electronics on one side and sufficiently away from of the robotic system. Finally, the complete sensing system is implemented and experimentally evaluated, resulting in a maximum error of 6° with respect to the used camera ground truth information in measuring the bending angle in individual segments. From the experimental results, it can be implied that the sensing error can be decreased by increasing the initial stretch length of recovery springs, to have a tighter cable system in low flexion. We have

also demonstrated the multi segment flex sensing exploiting collocation of passive cables in successive segments. This sensing system can be regarded as complimentary for the two-segment soft actuation system presented in [20, 21].

Future work will focus on further development of the flexible arm, by activating its internal actuation mechanism using actuating tendons and motors. Having installed actuators, we will have the opportunity to produce various motion patterns and characterise the entire sensing workspace.

REFERENCES

- [1] H. Yamada, S. Chigisaki, M. Mori, K. Takita, K. Ogami, S. Hirose, "Development of amphibious snake-like robot ACM-R5". Proc. 36th Int'l Symp. Robotics 36, 133, 2005.
- [2] K. Lipkin, I. Brown, A. Peck, H. Choset, J. Rembisz, P. Gianfortoni, A. Naaktgeboren. "Differentiable solution and piecewise differentiable gaits for snake robots". In Proc. IEEE Int'l Conference on Intelligent Robots and Systems, 1864 – 1869. San Diego, CA, 2007.
- [3] M. Calisti, M. Giorelli, G. Levy, B. Mazzolai, B. Hochner, C. Laschi, P. Dario "An octopus-bioinspired solution to movement and manipulation for soft robots". *Bioinspir Biomim.* 6(3):036002, 2011.
- [4] D. Trivedi, C. Rahn, W. Kier, I. Walker. "Soft robotics: biological inspiration, state of the art, and future research". *Appl. Bionics. Biomech.* 5, 99 – 117, 2008.
- [5] M. Cianchetti, T. Ranzani, G. Gerboni, I. De Falco, C. Laschi, A. Menciassi "STIFF-FLOP Surgical Manipulator: mechanical design and experimental characterization of the single module", *IEEE/RSJ Int'l Conference on Intelligent Robots and Systems (IROS)*, 2013.
- [6] J. Shang, D. Noonan, C. Payne, J. Clark, M. H. Sodergren, A. Darzi, G.-Z. Yang, "An Articulated Universal Joint Based Flexible Access Robot for Minimally Invasive Surgery", *IEEE Int'l Conference on Robotics and Automation*. pp. 1147-1152, 2011.
- [7] A. Degani, H. Choset, B. Zubiate, T. Ota and M. Zenati, "Highly Articulated Robotic Probe for Minimally Invasive Surgery," in 30th Annual Int'l IEEE EMBS Conference, Canada, August 2008.
- [8] OC Robotics, Snake-arm robots access the inaccessible", *OC Robotics, Nuclear Technology International*, 2008, p92-94.
- [9] S. Sareh, J.M. Rossiter, A.T. Conn, K. Drescher, R.E. Goldstein "Swimming like algae: biomimetic soft artificial cilia", *Journal of the Royal Society Interface* 20120666, 2013.
- [10] J.M. Croom, D.C. Rucker, J.M. Romano, R.J. Webster. "Visual sensing of continuum robot shape using self-organizing maps", *IEEE Int'l Conference on Robotics and Automation*, 4591 – 4596, 2010
- [11] M. Mahvash, and D.E. Dupont, "Stiffness Control of a Continuum Manipulator in Contact with a Soft Environment", *IEEE/RSJ Int'l Conference on Intelligent Robots and Systems 2010*:863-870, 2010.
- [12] A. Punning, M. Kruusmaa, & A. Abaloo, "Surface resistance experiments with IPMC". *Sensors and Actuators A*, 133(1), pp. 200-209, 2007.
- [13] S. Ryu, P. E. Dupont, "FBG-based Shape Sensing Tubes for Continuum Robots", *IEEE Int'l Conference on Robotics and Automation*, pp. 3531-3537, 2014.
- [14] X. Zhang, J.J.Max, X. Jiang, L. Yu, H. Kassi, "Experimental investigation on optical spectral deformation of embedded FBG sensors", *Proc. SPIE 6478, Photonics Packaging, Integration, and Interconnects VII*, 647808, 2007.
- [15] P. Polygerinos, L. D. Seneviratne, and K. Althoefer, "Modeling of Light Intensity-Modulated Fiber-Optic Displacement Sensors," *Actions on Instrumentation and Measurement*, vol. 60, no. 4, pp. 1408-1415, 2011.
- [16] P. Puangmali, H. Liu, L. D. Seneviratne, P. Dasgupta, K. Althoefer. "Miniature 3-axis distal force sensor for minimally invasive surgical palpation". *Mechatronics, IEEE/ASME Transactions on*, 17(4), pp: 646-656. 2012.
- [17] T.C. Searle, K. Althoefer, L.D. Seneviratne, H. Liu, "An optical curvature sensor for flexible manipulators". *ICRA 2013*: 4415-4420, 2013.
- [18] R. J. Webster III, and B. A. Jones, "Design and Kinematic Modeling of Constant Curvature Continuum Robots: A Review," *International Journal of Robotics Research*, vol. 29, no. 13, pp. 1661-1683, 2010.

- [19] P. Breedveld, J. Scheltes, E. Blom, and J. Verheij, "A New, Easily Miniaturized Steerable Endoscope," *IEEE Eng. Med. Biol. Mag.*, pp. 40–47. 26, 2005.
- [20] T. Ranzani, G. Gerboni, M. Cianchetti, A. Menciassi. "A bioinspired soft manipulator for minimally invasive surgery", *IOP Bioinspiration&Biomimetics*, Special issue on octopus inspired robots.
- [21] Y., Noh, S., Sareh, J., Back, H., Würdemann, T., Ranzani, E.L., Secco, A., Faragasso, H., Liu, K. Althoefer (2014) Development of a Three Axial Body Force Sensor for Flexible Manipulators, *IEEE Int'l Conference on Robotics and Automation (ICRA) 2014*.
- [22] S., Sareh, Y., Noh, T., Ranzani, H., Würdemann, H., Liu, K. Althoefer Modular fibre-optic shape sensor for articulated surgical instruments, *Hamlyn Symposium on Medical Robotics*, 2015.
- [23] S. Sareh, A.T. Conn and J. M. Rossiter, Optimization of bio-inspired multi-segment IPMC cilia EAPAD XII: *Proc. Electroactive Polymer Actuators and Devices vol 7642 SPIE*, 2010.